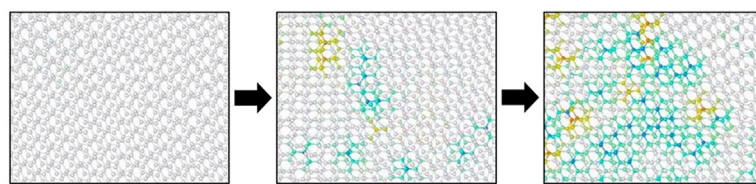
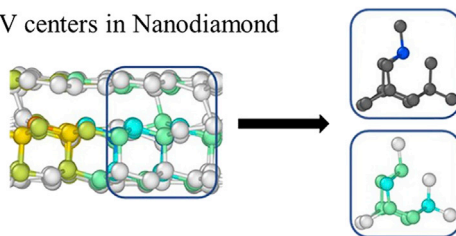


**Article**

# Molecular-Scale Nanodiamond with High-Density Color Centers Fabricated from Graphite by Laser Shocking



NV centers in Nanodiamond



## Evolution of high density NV centers in nanodiamonds after laser shock

Maithilee Motlag, Xingtao Liu,  
Ni Putu Dewi NurmalaSari, ...,  
Libai Huang, Jing Liu, Gary J.  
Cheng

urrliu@iupui.edu (J.L.)  
gjcheng@purdue.edu (G.J.C.)

### HIGHLIGHTS

Ultrafast laser shock is used to transform graphite to nanodiamonds at ambient conditions

The nanodiamonds can individually host ~100 NV centers

Annealing greatly enriches number of NV centers and enhances spontaneous decay rate

Motlag et al. describe an ultrafast laser shocking technique to obtain ultrahigh concentrations of color centers in nanodiamonds (~5 nm) under ambient conditions. Each nanodiamond can individually host ~100 NV centers, which is orders of magnitude higher than the state of the art.



Article

# Molecular-Scale Nanodiamond with High-Density Color Centers Fabricated from Graphite by Laser Shocking

Maithilee Motlag,<sup>1,2,6</sup> Xingtao Liu,<sup>1,2,6</sup> Ni Putu Dewi NurmalaSari,<sup>3,6</sup> Shengyu Jin,<sup>1,2,6</sup> Qiong Nian,<sup>2</sup> Charles Park,<sup>4</sup> Linrui Jin,<sup>5</sup> Libai Huang,<sup>5</sup> Jing Liu,<sup>4,\*</sup> and Gary J. Cheng<sup>1,2,7,\*</sup>

## SUMMARY

Nanodiamonds (NDs) with nitrogen vacancy (NV) color centers have the potential for quantum information science and bioimaging due to their stable and non-classical photon emission at room temperature. Large-scale fabrication of molecular-size nanodiamonds with sufficient color centers may economically promote their application in versatile multidisciplinary fields. Here, the manufacture of molecular-size NV center-enriched nanodiamonds from graphite powder is reported. We use an ultrafast laser shocking technique to generate intense plasma, which transforms graphite to nanodiamonds under the confinement layer. Molecular dynamics simulations suggest that the high pressure of 35 GPa and the high temperature of 3,000K result in the metaphase transition of graphite to nanodiamonds within 100 ps. A high concentration of NV centers is observed at the optimal laser energy of 3.82 GW/cm<sup>2</sup>, at which point molecular-size (~5 nm) nanodiamonds can individually host as many as 100 NV centers. Consecutive melamine annealing following ultrafast laser shocking enriches the number of NV centers >10-fold and enhances the spontaneous decay rate of the NV center by up to 5 times. Our work may enhance the feasibility of nanodiamonds for applications, including quantum information, electromagnetic sensing, bioimaging, and drug delivery.

## INTRODUCTION

The nitrogen vacancy (NV) center in diamonds has played an important role in quantum computing,<sup>1</sup> magnetic fields,<sup>2</sup> sensing nuclei,<sup>3–6</sup> and bioimaging.<sup>7,8</sup> The emerging nanometer-size diamond particles enriched by the NV centers have drawn much attention due to their unique optical properties.<sup>9–12</sup> Due to the long coherence time (~milliseconds at room temperature) of the electron spin states, the nanodiamond (ND) becomes sensitive to electric and magnetic fields. The ND is also a promising candidate in bioimaging and biomedicine due to features such as photoluminescence, biocompatibility, and flexible surface chemistry.<sup>13–16</sup> The outstanding photostability and brightness of the ND enable the longtime visualization of biological specimens with high temporal and spatial resolution. Meanwhile, the ND also exhibits great sensitivity to the magnetic field and acoustic waves, enabling it to be an excellent marker for electron imaging, nuclear magnetic resonance (NMR), and acoustic imaging. Such multimodal imaging biomarkers would ensure better elucidation of physiological mechanisms at molecular and cellular levels,<sup>17–19</sup> thus having an immensely beneficial role in the improved diagnosis and therapeutic management of a disease. Researchers have indicated that the

<sup>1</sup>School of Industrial Engineering, Purdue University, West Lafayette, IN 47907, USA

<sup>2</sup>Birck Nanotechnology Center, Purdue University, West Lafayette, IN 47907, USA

<sup>3</sup>Department of Nanoscience and Nanoengineering, South Dakota School of Mines and Technology, Rapid City, SD 57701, USA

<sup>4</sup>Department of Physics, Indiana University-Purdue University, Indianapolis, Indianapolis, IN 46202, USA

<sup>5</sup>Department of Chemistry, Purdue University, West Lafayette, IN 47907, USA

<sup>6</sup>These authors contributed equally

<sup>7</sup>Lead Contact

\*Correspondence: [urraliu@iupui.edu](mailto:urraliu@iupui.edu) (J.L.), [gjcheng@purdue.edu](mailto:gjcheng@purdue.edu) (G.J.C.)

<https://doi.org/10.1016/j.xcpr.2020.100054>



ND could also serve as the probe for imaging-guided drug delivery and that the efficiency of the drug delivery can be accelerated in cancer treatment and therapy.<sup>20</sup> Biomedical applications could substantially benefit from molecular-size NDs with abundant color centers. Reduction in the size of the NDs would facilitate cellular uptake and transportation in the vesicles and between organs, and would allow more sensitive detection of electromagnetic fields.

Alongside the conventional manufacturing approaches of NDs, such as ion implantation,<sup>2</sup> high pressure high temperature (HPHT),<sup>21</sup> and chemical vapor deposition (CVD),<sup>22</sup> great efforts have been made to fabricate or synthesize molecular-size (<5 nm) NDs.<sup>23,24</sup> NDs <5 nm have been produced by several bottom-up and top-down approaches; however, these fabrication methods are always limited by several factors such as high energy, high cost, extreme environments, and low yield.<sup>25–28</sup> In this report, we fabricate diamonds from graphite using a laser shocking technique at room temperature and atmospheric pressure. Melamine ( $C_3H_6N_6$ ), as the nitrogen source of the nitrogen (N)-doped ND, contains 6 C–N bonds, 3 C=N bonds, and 6 N–H bonds. Hydrogen is the only impurity in this organic molecule. Conventional detonation ND (DND) was produced by mixing graphite with explosive mixtures such as trinitrotoluene (TNT) or hexogen (RDX), which also contains oxygen as an impurity. Therefore, the content of the lower-impurity atoms makes melamine an ideal nitrogen source. Graphite spray-coated glass with a thin melamine layer and a glass slide were put on the top as the confinement layer. Then, the sample was exposed to a nanosecond-picosecond laser pulse that generated an intense thermal shock in a short time, leading to extreme environment close to isovolumetric process. Due to the increase in temperature, enormous pressure was generated, which transformed the carbon layer into a metastable carbon plasma plume formation, which in turn, formed a graphite-diamond phase.<sup>29</sup> This novel approach to fabricating NDs with NV centers has several advantages such as high-speed production, flexible processing, and low cost, without high temperature, high vacuum, and expensive laser.

It is essential for NV centers as single-photon sources to emit sufficient brightness at a fast rate.<sup>30</sup> To increase the sensitivity of the NV centers, they should be brought closer to the surface (<5 nm).<sup>31</sup> Some methods such as oxygen annealing and plasma treatment were applied to etch the surface of the diamond.<sup>32</sup> These techniques are difficult to control and can damage the surface of the diamond. Radiative decay has played an important role in the excited lifetime; consequently, reduction lifetimes of NV centers were reported by engineering the refractive index of the substrate,<sup>33</sup> manipulating the electromagnetic environment, or coupling with plasmonic material.<sup>34–37</sup> An electron-hole pair was produced by an energy transfer from the NV centers to graphene; as a result, there was a decrease in lifetime and intensity.<sup>35</sup> Here, we report our work on a fabrication protocol for NV centers from graphite by laser shaping. The size of the NDs is ~5 nm. We determined that the fluorescence decay times of the NV center were 2.6 and 3.5 ns with the melamine layer since the position of the NV center is closer to the surface. We observe that the melamine layer produces more NV centers due to an excess of nitrogen during laser ablation.

## RESULTS AND DISCUSSION

### Characterization of the As-Fabricated NDs

The ultrafast transition of N-doped graphite to the ND with color centers is enabled by a confined pulse laser deposition (CPLD) setup, as depicted in Figure 1. The mixture of graphite and melamine was deposited on the silica substrate in a sandwich structure with a transparent confinement layer on top. The ultrashort exposure

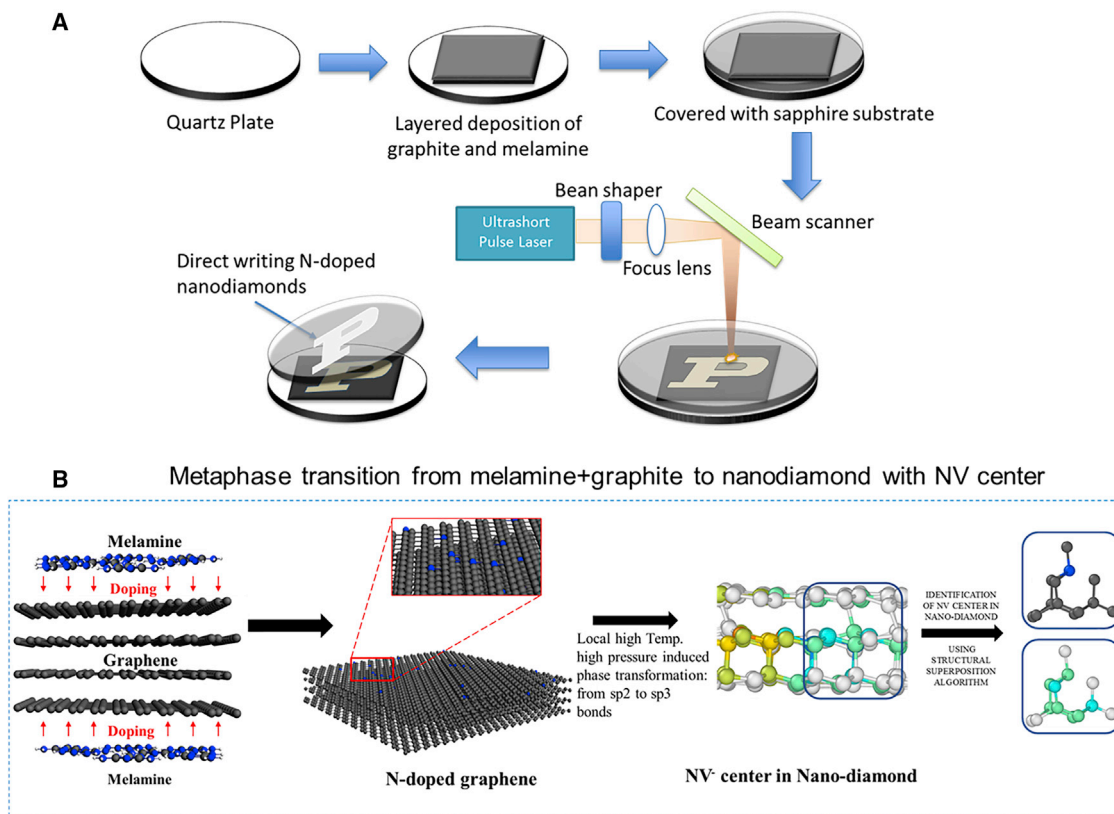


**Figure 1. Experimental Setup**

(A) Experimental setup of ultrafast metaphase transition of N-doped graphite to nanodiamonds (NDs) with color centers. N-doped graphene is obtained by mixing graphene and melamine.

(B) Illustration of metaphase transition from mixture of graphene and melamine to NDs with NV centers from molecular dynamics (MD) simulation.

of the high-energy laser pulses in such an extremely localized environment transforms the graphite composite to ND particles, inside which some carbon atoms were replaced by the defects, and the NV centers are formed. The inset of Figure 1 depicts the metaphase transition process, which is specifically discussed and validated via molecular dynamics (MD) simulations. In our work, we started from the laser intensity of  $\sim 1.91 \text{ GW/cm}^2$ , corresponding to a laser pulse energy of 300 mJ, and ended at  $\sim 5.73 \text{ GW/cm}^2$ , corresponding to a pulse energy of 900 mJ. It was found that all of the laser intensities led to ND crystals with distinguishable growth faces (Figures 2A and 2B). As marked in white arrows and dashed circles in Figures 2A and S1A, NDs  $\sim 5 \text{ nm}$  in diameter possess distinctive lattice structures as compared to the surrounding graphite; the size distribution is shown in Figure 2H. The lattice of the ND lattice is distorted since the ND is doped by nitrogen, which results in the formation of the NV color centers in the ND. As shown in a high-resolution transmission electron microscopy (HRTEM) image in Figures 2B and S1B, the lattice spaces (02-2) of 0.252 nm indicate the atomic arrangement of N-doped NDs along the [111] zone axis, while the interplanar space of the {110} family of the crystal plane in the single ND is 0.246 nm. Figure 2C shows the corresponding fast Fourier transform (FFT) image from Figure 2B. Atomic force microscopy (AFM) topography (Figures S5A and S5B) shows that the ND has a size of 5019 nm and uniformly distributed on the glass substrate. However, due to the inhomogeneity of the melamine distribution, the highly doped area has a higher fluorescence intensity, as shown in Figure S5C. Scanning transmission electron microscopy (STEM) and

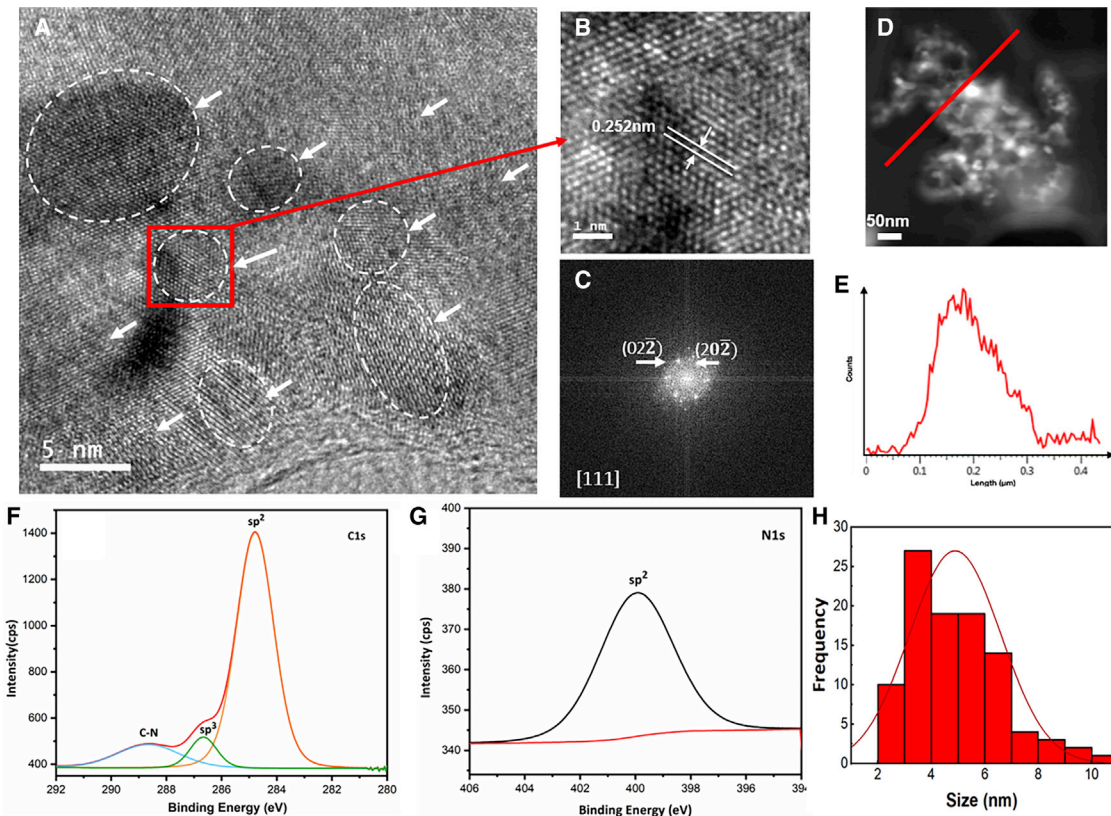


**Figure 2. Microstructural and Compositional Analysis of As-Fabricated NDs**

(A) HRTEM characterization of as-fabricated randomly oriented NDs. Scale bar, 5 nm.

(B) NDs oriented in  $[111]$  zone axis. Scale bar, 1 nm.

(C) FFT of the NDs shown in (B).

(D) High-angle annular dark-field imaging (HAADF)-STEM image of NDs. Scale bar, 50 nm.

(E) Nitrogen concentration along the line marked in (D) by EDS line scan.

(F and G) XPS characterization of NDs with C1s (F) and N1s (G).

(H) Size distribution of the nanodiamonds synthesized from laser shocking.

energy-dispersive spectroscopy (EDS) line scans were conducted to characterize the composition of the fabricated NDs, as presented in Figures 2D and 2E. The distribution of nitrogen was confirmed with the help of X-ray energy-dispersive spectroscopy, which is the direct evidence of the existence of nitrogen in NDs. Along the direction of the line scan, shown as the red line in Figure 2D, the concentration of nitrogen increases in the cluster of NDs. X-ray photoelectron spectroscopy (XPS) was performed to further confirm the composition of the NDs. C1s ( $sp^3$ ) from NDs was verified at 286.5 eV, and the C–N bond was observed at 288.5 eV, as seen in Figure 2F. The C1s XPS signal consists of 2 main peaks: one centered at 284.9 eV, corresponding to C–C bonds in the diamond matrix, and another peak centered at 287.3 eV, corresponding to C–N bonds. In addition, nitrogen binding was found at  $\sim$ 401.0 eV to verify the successful integration of the NV center into NDs.<sup>38</sup> The main peak of the N1s signal at  $\sim$ 401 eV corresponds to chemical bonds of the type N– $sp^3$ –C. This peak is a characteristic of interior elemental nitrogen covalently bound within the diamond lattice. Figure S2 shows the XPS analysis of carbon and nitrogen at 4 different sites. We can observe the formation of the C1s  $sp^3$  peak and the C1s C–N bonding peak, which prove that the NDs are successfully synthesized from graphite and that nitrogen is successfully doped in the sample. In our

XPS results, we tested the ND samples synthesized with different laser energies. The main peak of the N1s signal at ~401 eV corresponds to chemical bonds of the type N–sp<sup>3</sup>–C. This peak is a characteristic of interior elemental nitrogen covalently bound within the diamond lattice. The C1s XPS signal consists of 2 main peaks: one centered at 284.9 eV, corresponding to C–C bonds in the diamond matrix, and the other peak centered at 287.3 eV, corresponding to C–N bonds.<sup>39,40</sup> Among all of the XPS results, we can observe the formation of the C1s sp<sup>3</sup> peak and the C1s C–N bonding peak, which is another piece of evidence that the ND is successfully synthesized from graphite and that nitrogen is successfully doped in the sample. In addition, Raman spectroscopy in [Figure S6](#) also shows the formation of nanodiamond since the sp<sup>3</sup> bonded carbon contributes to the peak at 1347 cm<sup>-1</sup>.

The transformation of graphite-to-diamond has an intermediate phase of carbon vapors that distort the crystalline order of graphite and dramatically reduce the dynamic barrier for the diamond synthesis. The phase transition from the carbon vapor to graphite and diamond has equal probability due to the negligible energy differences.<sup>41</sup> Therefore, specific extreme conditions such as laser-induced plasma sources are required to enable the selective transition of carbon vapors to diamonds. Experimental studies performed at Los Alamos National Laboratory<sup>42,43</sup> suggest the transformation of graphite-to-diamond phase at temperatures of ~5,000 K and pressures of ~10 GPa. In our approach, the localized high pressure generated by the laser shock assists in the graphite-to-diamond phase transformation. The instantaneous increase of the temperature induced by the ultrafast laser pulses activates the formation of the carbon plasma plume in the sandwiched structure, leading to a large pressure. Meanwhile, the transparent confinement layer impedes the thermal expansion of the carbon vapor, leading to the extreme localized confinement, which further enhances the graphite-diamond transition. Nian et al. attained ND formation using a nanosecond laser ablation of graphite at lower pressures of 4.4 GPa due to localized high-density plasma resulting from the solid confinement.<sup>44</sup> Classical MD and *ab initio* simulations demonstrated the underlying mechanism of the kinetics of graphite-to-diamond phase conversion.<sup>45</sup> In this research, due to the localized high temperature and pressure generated by the laser, the ND thin film is fabricated on the confinement layer. Therefore, the method of laser-direct writing has the potential to scale the ND fabrication to 3-dimensional (3D) scale by using a 3D patterned confinement layer. The 3D pattern can be achieved by lithography, nanoimprinting, and e-beam lithography.

#### MD Simulation of Metastable Graphite-Diamond Phase Transition

As discussed in our prior work, the ultrafast laser pulse generates localized HPHT non-equilibrium conditions, which result in metaphase transformation.<sup>46</sup> The metaphase transition of graphite to ND consists of 3 major steps: plasma formation, plasma condensation, and ultrafast annealing. Here, we conducted *ab initio* simulations to mimic the transformation of the graphite to the diamond with high temporal resolution. Nanostructure evolution of the transformation was investigated using MD to an observed NV center in NDs under HPHT conditions using laser heating. Graphitic nitrogen was subjected to laser heating to observe the preferred site of the implantation of the NV center in NDs for the atomic configurations of the NV center in NDs. Graphene was doped with ~1% nitrogen due to excess nitrogen atoms from melamine resulting in N-doped graphite as seen in [Figure 3A](#). The system was first minimized using the conjugate gradient method followed by equilibration using the isothermal-isobaric (NPT) ensemble at a constant temperature of 300 K for 40 ps. The equilibrated configuration can be seen in [Figure 3B](#). Initiation of the nucleation of the diamond metastable phase was observed at ~60–70 ps and is denoted in [Figure 3C](#). A non-equilibrium structural metaphase transition of N-doped graphite to the N-doped metastable phase of cubic

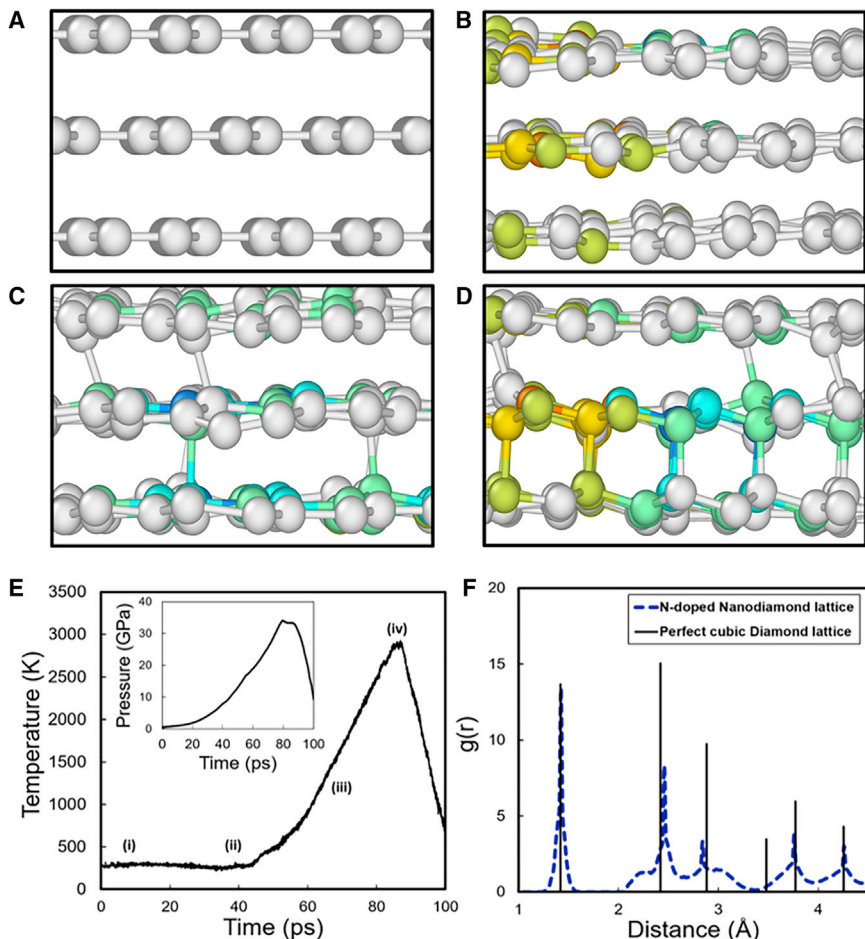


**Figure 3. MD Simulation of the Metaphase Transformation of Graphene to NDs**

(A) Initial configuration of 1% N-doped graphene. Gray represents the absence of cubic diamond structure before equilibration.

(B) Equilibrated configuration at 40 ps.

(C) Initiation of nucleation of diamond metastable phase under HPHT. Slight evidence of phase change is observed at ~60–70 ps.

(D) Structural transition of N-doped graphite to N-doped metastable phase of NDs observed at ~80–85 ps.

(E and F) Pressure and temperature profiles are shown for (A) and (B) as depicted by (i)–(iv) (E), and (F) shows the comparison of the radial distribution function of the NV center in NDs subjected to laser heating and the radial distribution function of perfect cubic diamond structure.

ND under a high localized pressure of ~34 GPa and high temperature conditions of 2,900K was observed at ~80–85 ps (Figure 3D). It was found that the formation of the NV<sup>-</sup> center in NDs was strongly dependent on the temperature and pressure conditions during laser heating. The corresponding pressure and temperature profiles are shown in Figure 3E. A substitutional site for nitrogen was generated due to the favorable temperature and pressure conditions that were associated with a vacancy. The process of the phase transformation is depicted in Videos S1 and S2. The presence of the NV center was located using a superposition search algorithm. The coordinates of a perfect N-doped ND structure with a vacancy (i.e., absence of a carbon atom adjacent to the nitrogen atom) was compared with the coordinates of the output data files generated from MD simulations to obtain a best fit<sup>6,47</sup> via the rotation and translation of matrices.

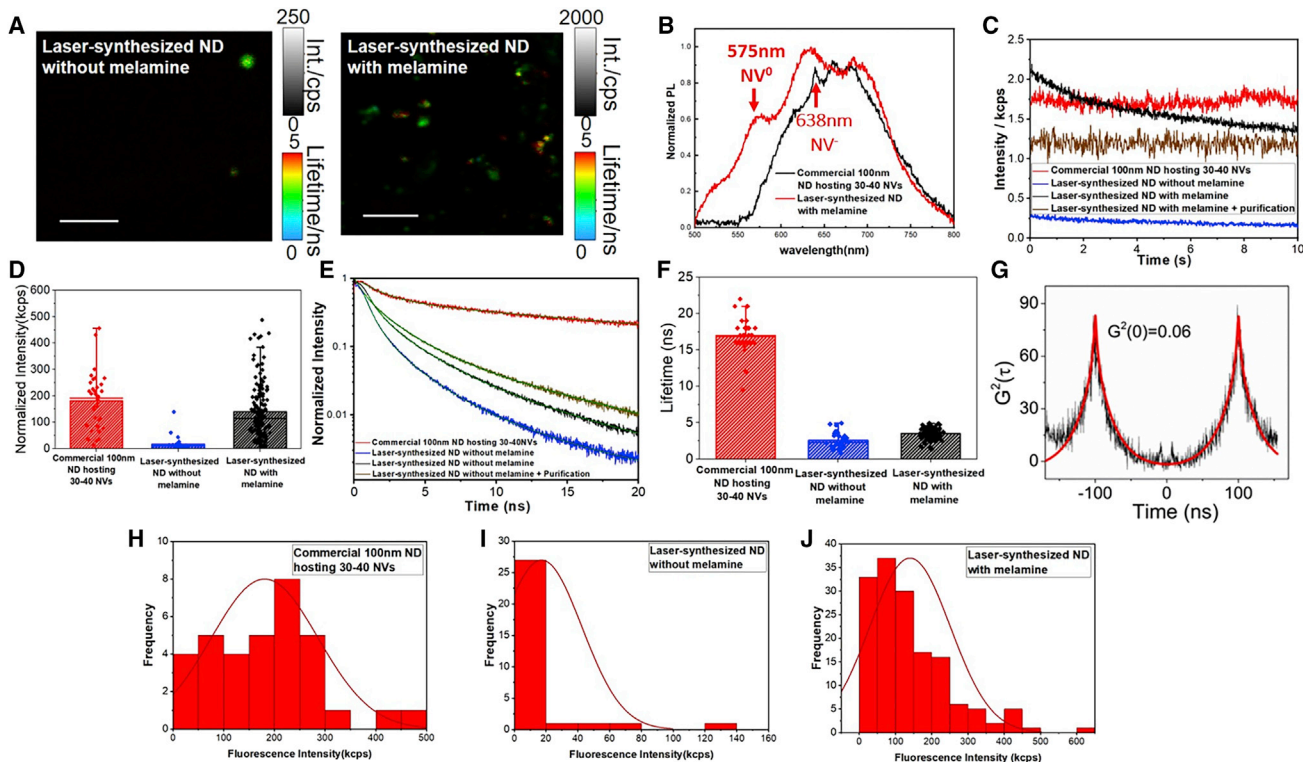


**Figure 4. Photon Emission Behaviors of the NV Center in Synthesized NDs**

(A) FLIM. Scale bar, 20 μm.  
(B–F) Photoluminescence (PL) spectrum showing the existence of NV centers (B), time-trace intensity (C), intensity distribution (D), time-correlated single photon counting (TCSPC) decay curves (E), and the mean lifetime distribution of NV centers with and without melamine and the commercial NDs (F).

(G) Antibunching measurement showing the evidence of single NV center photon emission.

(H–J) The histogram showing the distribution of fluorescence intensity. Error bars represent the standard error of the mean.

The structural characterization of the ND from the N-doped graphitic structure was further validated with the help of the radial distribution function. It is defined  $asg(r) = \frac{(n(r, \Delta r))}{(4\pi r^2 \Delta r)^3}$ , where  $(n(r, \Delta r))$  is the average number of atoms in a spherical shell of thickness  $\Delta r$  at distance  $r$  and  $4\pi r^2 \Delta r$  is the volume of the shell. The diamond structure has neighboring carbon atoms at characteristic distances, which makes it possible to identify the dynamic structural phase change from graphitic carbon to ND carbon. As observed from Figure 3F, the radial distribution function obtained from the simulations depict the first peak at a nearest-neighbor distance of 1.42 Å and the second peak at a nearest-neighbor distance of 2.46 Å, which agree with the radial distribution function of the perfect cubic diamond structure obtained from simulations<sup>48,49</sup> and experimental works.<sup>50,51</sup> The phase transition of N-doped graphite to the formation of the NV center in the ND structure using MD simulations is shown in Video S1.

#### Analysis of the Photon Emission Behavior of the NDs

The photon emission from the NV centers of the ND was characterized by time-resolved fluorescence microscopy. As shown in Figure 4, the addition of melamine in the graphite composite significantly enriches the NV centers in the synthesized ND, in which both the number and the brightness of the bright spot increase. Compared with the commercial HPHT NDs (100 nm), our NDs hold similar fluorescent spectrums with the zero-phonon line at 638 nm (Figure 4B), which confirms

the existence of the NV centers. Because of the different charge states of the NVs formed in ND, there are 2 peaks shown in the photoluminescence (PL) spectrum of NVs, NV<sup>-</sup> (638 nm) and NV<sup>0</sup> (575 nm), which are the zero-phonon bands of the 2 kinds of NV centers.<sup>52,53</sup> Both of the PL spectrums shown in Figure 4B showed the formation of the NV<sup>-</sup> and NV<sup>0</sup> in the commercial 100-nm NDs and the synthesized 5-nm NDs. Room temperature absorption spectrum of the ND-melamine sample shows a sharp peak at 636 nm, which shows the formation of NV<sup>-</sup>, as shown in Figure S7. However, due to the concentration, the charge state and position of the NVs in the 100-nm NDs and 5-nm NDs are different, and the intensity of the NV<sup>0</sup> peak (575 nm) and the NV<sup>-</sup> peak (638 nm) are different in the spectrums tested at different places in the as-fabricated sample. All of the spectrums show the same shape with different intensities, as seen in Figure S8. And because of the high concentration of the NV center in the as-fabricated NDs, there will be lattice distortion in the ND particles, which leads to different states between different NVs in ND particles. Therefore, during a PL characterization, the PL signal for each NV will have tiny differences and cause the broadening of the PL peaks.

Analysis of individual NDs has shown that the melamine coating between the graphite layer and the transparent layer allows for a higher concentration of nitrogen during laser shaping, which enhances the formation of NV centers. There is a >10-fold increase in the fluorescence intensity (Figures 4C and 4D) and a slight increase (2.6–3.5 ns) in the average fluorescence lifetime (Figures 4E and 4F). The average lifetime of a 20-nm ND is  $10.48 \pm 0.54$  ns (data not shown) and  $17.10 \pm 0.26$  ns for a 100-nm ND (Figures 4E and 4F). Figure 4C shows that the fluorescence intensity of the melamine-doped NDs decreases with time. This “photobleaching” effect is due to the energy transfer between NV centers and the surrounding graphite residues, which are located on the surface of the ND, with an average distance of 2.5 nm. The single NV center-hosted ND was acquired from the commercial ND hosts the single NV, ordered from Microdiamant AG (MSY 0.05, guaranteed agglomerate-free [GAF]). In addition, we have confirmed that most of the NV centers (>90%) are single NV centers by the 2nd-order correlation (antibunching) measurements, as shown in Figure 4G. According to the histogram shown in Figures 4H–4J, the fluorescence intensity of the commercial 100-nm NDs that host 30–40 NVs has a homogeneous distribution. In our investigation, the laser-synthesized NDs without melamine doping have a very low fluorescence intensity compared with the commercial 100-nm ND. When synthesizing the ND with melamine, the fluorescence intensity and distribution are shown to be in the same range as the commercial 100-nm ND, while the nanoparticle size is much smaller than the commercial ND. Therefore, by comparing the fluorescence intensity, we can conclude that the laser-synthesized NDs doped with melamine has the same number of NV centers as the commercial 100-nm NDs, while the size is only ~5 nm. The ND thin film is directly synthesized from graphite in a very short time, which is caused by the ultrafast laser. The NVs are not deeply diffused into the ND lattice, which results in the instability. One reason is that the ND is directly synthesized from the mixture of graphite and melamine, the impurities in the ND film will also bleach very fast when the film is exposed to laser during the test. After purification by placing the sample into perchloric acid at 200°C for 24 h, the photobleaching phenomenon disappears. Further purification of the sample by placing it in perchloric acid at 200°C for 24 h recovers the fluorescence intensity and leads to stable emission (Figure 4C; Video S3). The lifetime of the ND significantly decreased with the decreasing diameter of the ND particle. Compared to the commercial ND, there was a significant reduction in lifetime for the NV centers by laser shaping. This is due to the smaller size of the ND, which was found to be <5 nm, and that the NV center was closer to the surface of the ND. In addition, after purification, the lifetime of the NDs increased due to the removal of the graphite residue.

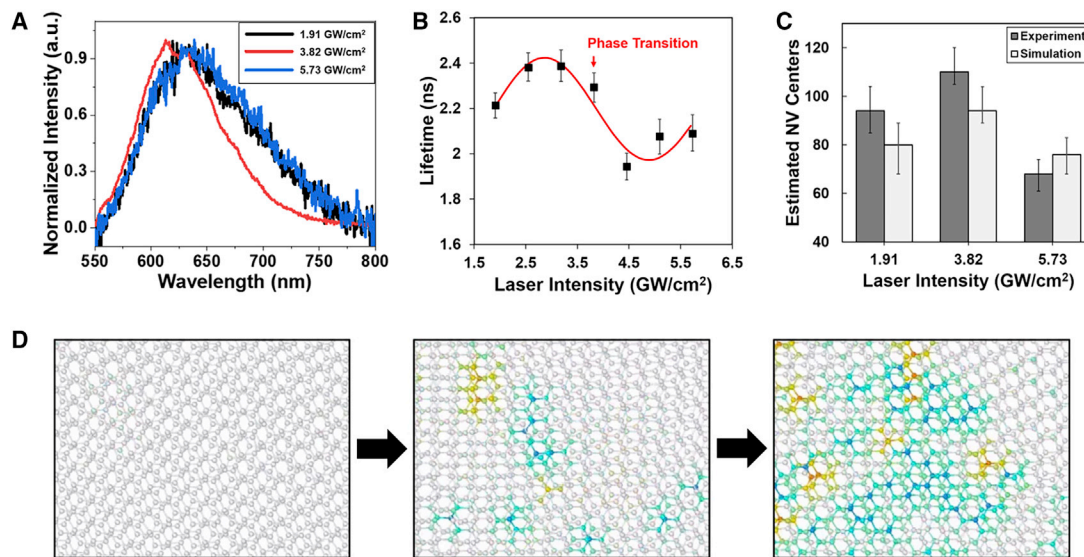


**Figure 5. Pulse Power-Dependent Photon Emission Behavior of the NDs**

(A) Spectrum of the NV center emission from the NDs shaped by 1.91 GW/cm<sup>2</sup>, 3.82 GW/cm<sup>2</sup>, and 5.73 GW/cm<sup>2</sup> laser energies.

(B) Fluorescence lifetime of individual NDs fabricated by different laser shaping powers.

(C) Calculated number of NV centers from the NDs shaped by 1.91 GW/cm<sup>2</sup>, 3.82 GW/cm<sup>2</sup>, and 5.73 GW/cm<sup>2</sup> laser energies.

(D) Snap shots from MD simulation on evolution of nanodiamond distribution in N-doped nanodiamonds.

Error bars represent the standard errors of the mean.

We also examined the photon emission from the ND sample with different laser-shaping intensities, from ~1.91 to ~5.73 GW/cm<sup>2</sup> (Figure 5). The NDs shaped by 1.91 GW/cm<sup>2</sup> and 5.73 GW/cm<sup>2</sup> power share similar spectral profiles, and the ND shaped by the 3.82 GW/cm<sup>2</sup> pulse has an obviously blue shift in the spectrum. This indicates that the NV centers in NDs shaped by 3.82 GW/cm<sup>2</sup> power have a larger band gap, which could originate from the larger lattice distance and may suggest phase transition at 3.82 GW/cm<sup>2</sup>. Previous studies<sup>54,55</sup> have shown a strong correlation in the sizes of the NDs and changes in band gap. As the size of the ND decreases, the band gap increases due to strong quantum confinement effects.<sup>56,57</sup> Due to high pressure, manipulation of the lattice structure and the electronic orbitals of the NV center is possible, resulting in a change in the band gap.<sup>58</sup> In addition, the pulse energy causes different laser-material interactions, which leads to a difference in the production rate of ND particles and the dopant concentration. Therefore, the band gap will change as well, which is reflected by the shifting of spectrums. This hypothesis is further supported by the summary of the lifetime of each pulse power, as shown in Figure 5B, in which a transition between 3.5 and 4 GW/cm<sup>2</sup> is observed. The NDs we synthesized in the study generally have a large number of NVs, leading to high fluorescence intensity. However, due to the nonuniformity of the melamine in the original graphite, the position, number, and charge state of the NV vary significantly in each single ND particle. The original lifetime distributions of the NV centers in NDs synthesized by different laser intensities are shown in Figure S9.

#### Pulse Power-Dependent Photon Emission Behavior of the ND

Figure 5C depicts the calculated number of NV centers from the ND shaped at 3 different laser energies: 1.91 GW/cm<sup>2</sup>, 3.82 GW/cm<sup>2</sup>, and 5.73 GW/cm<sup>2</sup>. The number of NV centers in each ND was calculated by normalizing the fluorescence intensity of each spot obtained in Figure 4A to the intensity of a single NV center. By

synthesizing the ND with different laser pulse energies, we have found that a pulse laser intensity of  $3.82 \text{ GW/cm}^2$  is the most optimal condition to synthesize NDs with high concentrations of NVs, which are due to the higher availability of substitutional sites for nitrogen atoms at the optimal temperature and pressure conditions as observed from the experiment and simulations. Either too high or too low levels of energy are not beneficial for the formation of NVs in NDs. This also corresponds to the phase transition observed in [Figures 5A and 5B](#). Therefore, the melamine produces a high concentration of nitrogen during laser ablation, which leads to stable  $\text{NV}^-$  near the surface. In addition, the presence of graphite allows the energy transfer from the NV center to graphene, producing 1 electron-hole pair,<sup>35</sup> which influences the fluorescence behavior of NV centers. The schematic process of MD simulations is explained in [Figure S3](#). MD simulations were performed using a large-scale atomic-molecular massively parallel simulator (LAMMPS)<sup>59</sup> to study the nanostructure evolution of N-doped NDs using laser heating to observe NV centers under high pressure. The estimated number of NV centers in the simulation was calculated using the structure superposition algorithm at different laser powers. The theoretical maximum number of NV centers was calculated statistically and was found to be  $\approx 132$ , as explained in [Data S1](#). The magnified top-view snapshots of the simulation that illustrate the phase change of N-doped graphite to N-doped NDs are shown in [Figure 5D](#). The identification of NV centers in N-doped NDs was made using structural superposition, and the close-up snapshot of the presence of the NV center using MD simulations is depicted in [Figure S4](#). The laser shock-induced formation of N-doped NDs is illustrated in [Video S1](#).

Studies about ND synthesis, fluorescent NDs, and NV centers created by irradiation damage using conventional fabrication<sup>60–63</sup> and by irradiation<sup>26,64–69</sup> has been compared with our work. Some of the referenced works created only a single NV center per crystal<sup>64–66</sup> or did not provide information regarding the concentration in parts per million.<sup>26,52,62,67</sup> In such cases, the concentration was calculated assuming a spherical crystal of a given diameter consisting of carbon atoms. Based on the existing literature, we have found that our method can produce an  $\sim 2\text{--}3$  orders of magnitude higher concentration of NV centers compared to the other methods.

In this report, we have proven that the NV center produced using the laser shaping technique could increase the rate of photon emission by decreasing the lifetime. The simulations can mimic the formation of nitrogen defects in the ND with the assumption that excess nitrogen from melamine is already doped with graphene, as seen in [Video S4](#). The number of NV centers in the computation cells can be seen in green in the video. The details of the simulation are discussed in [Data S1](#). The choice of the bond potential used in the MD simulations allows the study of effective chemical bonding and re-bonding. Thus, using our efficient approach, the NV fluorescent centers are created simultaneously during the fabrication process, reducing both time and cost and eliminating the extra irradiation process as in other fluorescent ND manufacturing methods.

In summary, we report a novel and low-cost approach to the large-scale fabrication of molecular-size NDs from graphite. The laser shaping method uses high-power laser pulses to induce plasma in extremely localized confinement to assist in the graphite-to-ND phase transition. This method leads to NDs of  $\sim 5 \text{ nm}$  hosting  $>100$  NV centers. Our experimental results are endorsed by the MD simulations.

## EXPERIMENTAL PROCEDURES

### MD Simulations

Non-equilibrium MD simulations were carried out to simulate the laser heating process using LAMMPS. Three types of interaction potentials were defined in this simulation: Tersoff potential to describe the covalent nature of C–C bonds,<sup>70</sup> Tersoff potential for covalent C–N bonds extracted from studies carried out by Matsunaga et al.,<sup>71</sup> and Lennard-Jones potential for depicting the Van der Waals interactions between non-bonded carbon atoms in different atomic planes. Periodic boundary conditions were imposed in X and Y directions. Laser heating was simulated by adding heat flux with an NVE ensemble. Non-equilibrium phase transition of graphitic layers to the cubic diamond was observed during the heating process. The phase transition was confirmed using the radial distribution function to compare the peaks of the perfect cubic diamond lattice structure with the laser-heated N-doped ND structure (see also Data S1).

### Fabrication of ND from Graphite

In this study, we fabricated two samples with and without melamine on sandwiched graphite between the backing plate and the quartz slide. The coating of graphite onto the backing plate was achieved by spraying aerosol graphite lubricant (Asbury Carbons) with a thickness of ~1–10 µm. Melamine was coated on top of the graphite in one sample, then the quartz slide was used as a confinement layer during laser shaping. A short pulse of the 248-nm KrF Excimer was used as laser power (Figure 1). The pulse laser power, ranging from 1.91 to ~5.73 GW/cm<sup>2</sup>, was applied to create 9 spots containing NV centers. The pulse duration of the laser was 5 ns, and the focused spot was ~3 mm. Melamine was coated on the sample to create excess nitrogen during laser ablation to increase the formation of the NV centers. The details of the CPLD process can be found in Reference 29. For reference and comparative purposes, aqueous commercial NDs with diameters of 20 and 100 nm (Microdiamant AG) were used in this study. A 20-µL ND solution was spin coated at 2,000 rpm for 2 min on a glass substrate (Corning; cover glass no. 1).

### Time-Resolved Fluorescence Microscopy

The study was performed using home-built confocal microscopy integrated with fluorescence lifetime imaging (FLIM, PicoQuant) (Figure 2). The fluorescence lifetime of the NV centers was collected using time-correlated scanning confocal microscopy (MicroTime 200, PicoQuant). A picosecond pulsed laser beam at 532 nm with a repetition frequency of 20 MHz was used for excitation. The lifetimes of fluorescence from NV centers were calculated based on fitting the spontaneous decay curves of NV centers. The emission spectra of NV centers were collected via an oil objective (100×, numerical aperture [NA] 1.4) for commercial NDs and an air objective (20×, NA 0.5) for NV centers by laser shaping by using QEPro (Ocean Optic).

## DATA AND CODE AVAILABILITY

All data are available from the Lead Contact upon reasonable request.

## SUPPLEMENTAL INFORMATION

Supplemental Information can be found online at <https://doi.org/10.1016/j.xcrp.2020.100054>.

## ACKNOWLEDGMENTS

G.J.C. acknowledges financial support from the National Institute of Standards and Technology (NIST) Intelligent Systems Division, National Science Foundation (NSF)

(CMMI 1741100) and the Office of Naval Research NEPTUNE program. L.H. and L.J. acknowledge support from the U.S. Department of Energy through award DE-SC0019215.

## AUTHOR CONTRIBUTIONS

G.J.C. conceived the idea of the synthesis technique and designed the experimental investigations. J.L. oversaw the characterization of the NDs with color centers. X.L., S.J., and Q.N. performed the experiments to synthesize the NDs with NV centers. M.M. conducted the simulation of the synthesis process and the comparison of the simulation with experimental results. S.J., X.L., N.P.D.N., L.J., and L.H. contributed to the characterization of the material. G.J.C., J.L., X.L., and M.M. analyzed the data and wrote the paper.

## DECLARATION OF INTERESTS

This work is protected by a US patent, publication number US20110210479 A1.

Received: November 15, 2019

Revised: February 17, 2020

Accepted: March 18, 2020

Published: May 6, 2020

## REFERENCES

- Holt, K.B. (2007). Diamond at the nanoscale: applications of diamond nanoparticles from cellular biomarkers to quantum computing. *Philos. Trans. R. Soc. A Math. Phys. Eng. Sci.* **365**, 2845–2861.
- Meijer, J., Burchard, B., Domhan, C., Wittmann, C., Gaebel, T., Popa, I., Jelezko, F., and Wrachtrup, J. (2005). Generation of single color centers by focused nitrogen implantation. *Appl. Phys. Lett.* **87**, 261909.
- Lithoxoos, G.P., Samios, J., and Carissan, Y. (2008). Investigation of silicon model nanotubes as potential candidate nanomaterials for efficient hydrogen storage: a combined ab initio/grand canonical Monte Carlo simulation study. *J. Phys. Chem. C* **112**, 16725–16728.
- Staudacher, T., Shi, F., Pezzagna, S., Meijer, J., Du, J., Meriles, C.A., Reinhard, F., and Wrachtrup, J. (2013). Nuclear magnetic resonance spectroscopy on a (5-nanometer)3 sample volume. *Science* **339**, 561–563.
- Mamin, H.J., Kim, M., Sherwood, M.H., Rettner, C.T., Ohno, K., Awschalom, D.D., and Rugar, D. (2013). Nanoscale nuclear magnetic resonance with a nitrogen-vacancy spin sensor. *Science* **339**, 557–560.
- Collins, A., Cooper, R.I., and Watkin, D.J. (2006). Structure matching: measures of similarity and pseudosymmetry. *J. Appl. Crystallogr.* **39**, 842–849.
- Balasubramanian, G., Lazariev, A., Arumugam, S.R., and Duan, D.W. (2014). Nitrogen-Vacancy color center in diamond-emerging nanoscale applications in bioimaging and biosensing. *Curr. Opin. Chem. Biol.* **20**, 69–77.
- Prabhakar, N., and Rosenholm, J.M. (2019). Nanodiamonds for advanced optical bioimaging and beyond. *Curr. Opin. Colloid Interface Sci.* **39**, 220–231.
- Hui, Y.Y., Cheng, C.-L., and Chang, H.-C. (2010). Nanodiamonds for optical bioimaging. *J. Phys. D Appl. Phys.* **43**, 374021.
- Kratochvílová, I., Kovalenko, A., Fendrych, F., Petráková, V., Záliš, S., and Nesládečka, M. (2011). Tuning of nanodiamond particles' optical properties by structural defects and surface modifications: DFT modelling. *J. Mater. Chem.* **21**, 18248–18255.
- Aharonovich, I., Castelletto, S., Simpson, D.A., Su, C.-H., Greentree, A.D., and Prawer, S. (2011). Diamond-based single-photon emitters. *Rep. Progr. Phys.* **74**, 076501.
- Aharonovich, I., Greentree, A.D., and Prawer, S. (2011). Diamond photonics. *Nat. Photonics* **5**, 397.
- Hui, Y.Y., Cheng, C.L., and Chang, H.C. (2010). Nanodiamonds for optical bioimaging. *J. Phys. D Appl. Phys.* **43**, 374021.
- Montalti, M., Cantelli, A., and Battistelli, G. (2015). Nanodiamonds and silicon quantum dots: ultrastable and biocompatible luminescent nanoprobes for long-term bioimaging. *Chem. Soc. Rev.* **44**, 4853–4921.
- von Haartman, E., Jiang, H., Khomich, A.A., Zhang, J., Burikov, S.A., Dolenko, T.A., Ruokolainen, J., Gui, H., Shenderova, O.A., Vlasov, I.I., and Rosenholm, J.M. (2013). Core-shell designs of photoluminescent nanodiamonds with porous silica coatings for bioimaging and drug delivery I: fabrication. *J. Mater. Chem. B Mater. Biol. Med.* **1**, 2358–2366.
- Khalid, A., Mitropoulos, A.N., Marelli, B., Simpson, D.A., Tran, P.A., Omenetto, F.G., and Tomljenovic-Hanic, S. (2015). Fluorescent nanodiamond silk fibroin spheres: advanced nanoscale bioimaging tool. *ACS Biomater. Sci. Eng.* **1**, 1104–1113.
- Merchant, K., and Sarkar, S.K. (2015). Fluorescent Nanodiamonds for molecular and cellular bioimaging. *IEEE J. Sel. Top. Quantum Electron.* **22**, 235–245.
- Hemelaar, S.R., de Boer, P., Chipaux, M., Zuidema, W., Hamoh, T., Martinez, F.P., Nagl, A., Hoogenboom, J.P., Giepmans, B.N.G., and Schirhagl, R. (2017). Nanodiamonds as multipurpose labels for microscopy. *Sci. Rep.* **7**, 720.
- Prabhakar, N., Peurla, M., Koho, S., Deguchi, T., Näröaja, T., Chang, H.C., Rosenholm, J.M., and Hänninen, P.E. (2018). STED-TEM Correlative Microscopy Leveraging Nanodiamonds as Intracellular Dual-Contrast Markers. *Small* **14**, 1701807.
- Ansari, S.A., Satar, R., Jafri, M.A., Rasool, M., Ahmad, W., and Kashif Zaidi, S. (2016). Role of nanodiamonds in drug delivery and stem cell therapy. *Iran. J. Biotechnol.* **14**, 130–141.
- Irifune, T., Kurio, A., Sakamoto, S., Inoue, T., and Sumiya, H. (2003). Correction: ultrahard polycrystalline diamond from graphite. *Nature* **421**, 806, 806.
- Yan, C.S., Mao, H.K., Li, W., Qian, J., Zhao, Y., and Hemley, R.J. (2004). Ultrahard diamond single crystals from chemical vapor deposition. *Physica Status Solidi A* **201**, R25–R27.
- Vlasov, I.I., Shiryaev, A.A., Rendler, T., Steinert, S., Lee, S.Y., Antonov, D., Vörös, M., Jelezko, F., Fisenko, A.V., Semjonova, L.F., et al. (2014). Molecular-sized fluorescent nanodiamonds. *Nat. Nanotechnol.* **9**, 54–58.
- Stehlik, S., Varga, M., Ledinsky, M., Miliaeva, D., Kozak, H., Skakalova, V., Mangler, C., Pennycook, T.J., Meyer, J.C., Kromka, A., and

- Rezek, B. (2016). High-yield fabrication and properties of 1.4 nm nanodiamonds with narrow size distribution. *Sci. Rep.* 6, 38419.
25. Morita, Y., Takimoto, T., Yamanaka, H., Kumekawa, K., Morino, S., Aonuma, S., Kimura, T., and Komatsu, N. (2008). A facile and scalable process for size-controllable separation of nanodiamond particles as small as 4 nm. *Small* 4, 2154–2157.
26. Mahfouz, R., Floyd, D.L., Peng, W., Choy, J.T., Loncar, M., and Bakr, O.M. (2013). Size-controlled fluorescent nanodiamonds: a facile method of fabrication and color-center counting. *Nanoscale* 5, 11776–11782.
27. Zhou, Y., Zhao, M., Adamo, G., Bauerick, S., Rudzinski, A., Aharonovich, I., and Gao, W. (2018). Direct writing of single germanium vacancy center arrays in diamond. *New J. Phys.* 20, 125004.
28. Chen, Y.-C., Salter, P.S., Knauer, S., Weng, L., Frangescou, A.C., Stephen, C.J., Dolan, P.R., Johnson, S., Green, B., Morley, G.W., et al. (2017). Laser writing of coherent colour centres in diamond. *Nat. Photonics* 11, 77–80.
29. Wang, C.X., Liu, P., Cui, H., and Yang, G.W. (2005). Nucleation and growth kinetics of nanocrystals formed upon pulsed-laser ablation in liquid. *Appl. Phys. Lett.* 87, 201913.
30. Eisaman, M.D., Fan, J., Migdall, A., and Polyakov, S.V. (2011). Invited review article: single-photon sources and detectors. *Rev. Sci. Instrum.* 82, 071101.
31. Ohashi, K., Rosskopf, T., Watanabe, H., Loretz, M., Tao, Y., Hauert, R., Tomizawa, S., Ishikawa, T., Ishi-Hayase, J., Shikata, S., et al. (2013). Negatively charged nitrogen-vacancy centers in a 5 nm thin 12C diamond film. *Nano Lett.* 13, 4733–4738.
32. Cui, S., Greenspon, A.S., Ohno, K., Myers, B.A., Jayich, A.C., Awschalom, D.D., and Hu, E.L. (2015). Reduced plasma-induced damage to near-surface nitrogen-vacancy centers in diamond. *Nano Lett.* 15, 2887–2891.
33. Tuna, M., Chavez-Reyes, A., and Tari, A.M. (2005). HER2/neu increases the expression of Wilms' Tumor 1 (WT1) protein to stimulate S-phase proliferation and inhibit apoptosis in breast cancer cells. *Oncogene* 24, 1648–1652.
34. Huck, A., Kumar, S., Shakoor, A., and Andersen, U.L. (2011). Controlled coupling of a single nitrogen-vacancy center to a silver nanowire. *Phys. Rev. Lett.* 106, 096801.
35. Liu, X., Wanga, G., Song, X., Feng, F., Zhu, W., Lou, L., Wang, J., Wang, H., and Bao, P. (2012). Energy transfer from a single nitrogen-vacancy center in nanodiamond to a graphene monolayer. *Appl. Phys. Lett.* 101, 233112.
36. Reserbat-Plantey, A., Schädler, K.G., Gaudreau, L., Navickaite, G., Güttinger, J., Chang, D., Toninelli, C., Bachtold, A., and Koppens, F.H. (2016). Electromechanical control of nitrogen-vacancy defect emission using graphene NEMS. *Nat. Commun.* 7, 10218.
37. Englund, D., Shields, B., Rivoire, K., Hatami, F., Vučković, J., Park, H., and Lukin, M.D. (2010). Deterministic coupling of a single nitrogen vacancy center to a photonic crystal cavity. *Nano Lett.* 10, 3922–3926.
38. Haque, A., and Sumaiya, S. (2017). An overview on the formation and processing of nitrogen-vacancy photonic centers in diamond by ion implantation. *J. Manuf. Mater. Process.* 1, 6.
39. Tjandra, R., Liu, W., Lim, L., and Yu, A. (2018). Melamine based, n-doped carbon/reduced graphene oxide composite foam for Li-ion hybrid supercapacitors. *Carbon* 129, 152–158.
40. Su, L.-X., Huang, Q.-Z., Lou, Q., Liu, Z.-Y., Sun, J.-L., Zhang, Z.-T., Qin, S.-R., Li, X., Zang, J.-H., Dong, L., and Shan, C.-X. (2018). Effective light scattering and charge separation in nanodiamond@ $\text{g-C}_3\text{N}_4$  for enhanced visible-light hydrogen evolution. *Carbon* 139, 164–171.
41. Mitra, S. (2004). *High Pressure Geochemistry & Mineral Physics: Basics for Planetary and Geo-Material Science* (Elsevier).
42. Mitchell, A.C., Shaner, J.W., and Keeler, R.N. (1986). The use of electrical conductivity experiments to study the phase diagram of carbon. *Physica B+C* 139, 386–389.
43. Shaner, J.W., Brown, J., Swenson, C., and McQueen, R. (1984). Sound velocity of carbon at high pressures. *J. Phys. Colloq.* 45, C235–C237.
44. Nian, Q., Wang, Y., Yang, Y., Li, J., Zhang, M.Y., Shao, J., Tang, L., and Cheng, G.J. (2014). Direct laser writing of nanodiamond films from graphite under ambient conditions. *Sci. Rep.* 4, 6612.
45. Xie, H., Yin, F., Yu, T., Wang, J.T., and Liang, C. (2014). Mechanism for direct graphite-to-diamond phase transition. *Sci. Rep.* 4, 5930.
46. Qiu, G., Nian, Q., Motlag, M., Jin, S., Deng, B., Deng, Y., Charnas, A.R., Ye, P.D., and Cheng, G.J. (2018). Ultrafast Laser-Shock-Induced Confined Metaphase Transformation for Direct Writing of Black Phosphorus Thin Films. *Adv. Mater.* 30, 1704405.
47. Diamond, R. (1990). Chirality in rotational superposition. *Acta Crystallogr. A* 46, 423.
48. Adiga, S.P., Adiga, V.P., Carpick, R.W., and Brenner, D.W. (2011). Vibrational properties and specific heat of ultrananocrystalline diamond: molecular dynamics simulations. *J. Phys. Chem. C* 115, 21691–21699.
49. Silverman, A., Adler, J., and Kalish, R. (2011). Diamond membrane surface after ion-implantation-induced graphitization for graphite removal: Molecular dynamics simulation. *Phys. Rev. B* 83, 224206.
50. Ren, W., Iyer, A., Koskinen, J., Kaskela, A., Kauppinen, E.I., Avchaviov, K., and Nordlund, K. (2015). Conditions for forming composite carbon nanotube-diamond like carbon material that retain the good properties of both materials. *J. Appl. Phys.* 118, 194306.
51. , S. Mitra, ed. (2013). *Physics of Structurally Disordered Solids Volume 20* (Springer Science & Business Media).
52. Chang, Y.-R., Lee, H.Y., Chen, K., Chang, C.C., Tsai, D.S., Fu, C.C., Lim, T.S., Tzeng, Y.K., Fang, C.Y., Han, C.C., et al. (2008). Mass production and dynamic imaging of fluorescent nanodiamonds. *Nat. Nanotechnol.* 3, 284–288.
53. Babinec, T.M., Hausmann, B.J.M., Khan, M., Zhang, Y., Maze, J.R., Hemmer, P.R., and Lončar, M. (2010). A diamond nanowire single-photon source. *Nat. Nanotechnol.* 5, 195.
54. Fokin, A.A., and Schreiner, P.R. (2009). Band gap tuning in nanodiamonds: first principle computational studies. *Mol. Phys.* 107, 823–830.
55. Hu, W., Li, Z., and Yang, J. (2013). Surface and size effects on the charge state of NV center in nanodiamonds. *Comput. Theor. Chem.* 1021, 49–53.
56. Bolker, A., Saguy, C., Tordjman, M., and Kalish, R. (2013). Quantum confinement and Coulomb blockade in isolated nanodiamond crystallites. *Phys. Rev. B* 88, 035442.
57. Raty, J.-Y., Galli, G., Bostedt, C., Van Buuren, T.W., and Terminello, L.J. (2003). Quantum confinement and fullerene-like surface reconstructions in nanodiamonds. *Phys. Rev. Lett.* 90, 037401.
58. Doherty, M.W., Struzhkin, V.V., Simpson, D.A., McGuinness, L.P., Meng, Y., Stacey, A., Karle, T.J., Henley, R.J., Manson, N.B., Hollenberg, L.C., and Prawer, S. (2014). Electronic properties and metrology applications of the diamond NV-center under pressure. *Phys. Rev. Lett.* 112, 047601.
59. Plimpton, S. (1995). Fast parallel algorithms for short-range molecular dynamics. *J. Comput. Phys.* 117, 1–19.
60. Eidelman, E.D., Siklitsky, V.I., Sharonova, L.V., Yagovkina, M.A., Ya Vul', A., Takahashi, M., Inakuma, M., Ozawa, M., and Ōsawa, E. (2005). A stable suspension of single ultrananocrystalline diamond particles. *Diam. Relat. Mater.* 14, 1765–1769.
61. Hsiao, W.W.-W., Hui, Y.Y., Tsai, P.C., and Chang, H.C. (2016). Fluorescent nanodiamond: a versatile tool for long-term cell tracking, super-resolution imaging, and nanoscale temperature sensing. *Acc. Chem. Res.* 49, 400–407.
62. Shenderova, O.A., Vlasov, I.I., Turner, S., Van, Tendeloo, G., Orlinskii, S.B., Shiryaev, A.A., Khomich, A.A., Sulyanov, S.N., Jelezko, F., and Wrachtrup, J. (2011). Nitrogen control in nanodiamond produced by detonation shock-wave-assisted synthesis. *J. Phys. Chem. C* 115, 14014–14024.
63. Rabeau, J.R., Stacey, A., Rabeau, A., Prawer, S., Jelezko, F., Mirza, I., and Wrachtrup, J. (2007). Single nitrogen vacancy centers in chemical vapor deposited diamond nanocrystals. *Nano Lett.* 7, 3433–3437.
64. Tisler, J., Balasubramanian, G., Naydenov, B., Kolesov, R., Grotz, B., Reuter, R., Boudou, J.P., Curni, P.A., Sennour, M., Thorel, A., et al. (2009). Fluorescence and spin properties of defects in single digit nanodiamonds. *ACS Nano* 3, 1959–1965.
65. Smith, B.R., Inglis, D.W., Sandnes, B., Rabeau, J.R., Zyagin, A.V., Gruber, D., Noble, C.J., Vogel, R., Osawa, E., and Plakhotnik, T. (2009). Five-nanometer diamond with luminescent nitrogen-vacancy defect centers. *Small* 5, 1649–1653.
66. Sonnefraud, Y., Cuche, A., Faklaris, O., Boudou, J.P., Sauvage, T., Roch, J.F., Treussart, F., and Huant, S. (2008). Diamond nanocrystals hosting single nitrogen-vacancy

- color centers sorted by photon-correlation near-field microscopy. *Opt. Lett.* 33, 611–613.
67. Fu, C.-C., Lee, H.Y., Chen, K., Lim, T.S., Wu, H.Y., Lin, P.K., Wei, P.K., Tsao, P.H., Chang, H.C., and Fann, W. (2007). Characterization and application of single fluorescent nanodiamonds as cellular biomarkers. *Proc. Natl. Acad. Sci. USA* 104, 727–732.
68. Faklaris, O., Garrot, D., Joshi, V., Druon, F., Boudou, J.P., Sauvage, T., Georges, P., Curmi, P.A., and Treussart, F. (2008). Detection of single photoluminescent diamond nanoparticles in cells and study of the internalization pathway. *Small* 4, 2236–2239.
69. Yu, S.-J., Kang, M.W., Chang, H.C., Chen, K.M., and Yu, Y.C. (2005). Bright fluorescent nanodiamonds: no photobleaching and low cytotoxicity. *J. Am. Chem. Soc.* 127, 17604–17605.
70. Tersoff, J. (1988). New empirical approach for the structure and energy of covalent systems. *Phys. Rev. B* 37, 6991.
71. Matsunaga, K., Fisher, C., and Matsubara, H. (2000). Tersoff potential parameters for simulating cubic boron carbonitrides. *Jpn. J. Appl. Phys.* 39, L48.